Electronic Supplementary Material (ESI) for Journal of Materials Chemistry A.

Supplementary Information

Tuning Thermal Storage Capacity and Flexibility of Solid-Solid Phase Change Materials towards Wearable Application

Jinming Shi,[a] Waseem Aftab,[a] Zibin Liang,[a] Kunjie Yuan,[a] Muhammad Maqbool,[a] Haoyang Jiang,[a] Feng Xiong, [a] Mulin Qin,[a] Song Gao,[a] and Ruqiang Zou[a]*

[a] Beijing Key Laboratory for Theory and Technology of Advanced Battery Materials, Department of Materials Science and Engineering, College of Engineering, Peking University, Beijing 100871, China. Email: rzou@pku.edu.cn

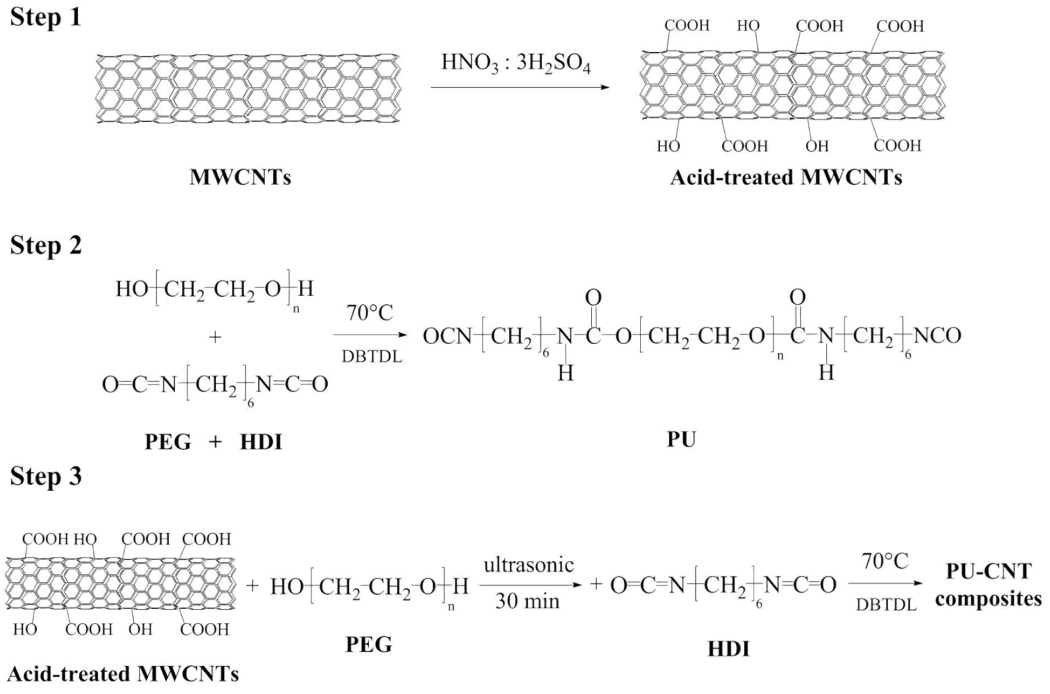

Scheme S1. Synthesis and Fabrication Process of the Acid-treated MWCNTs (Step 1), PU (Step 2), and PU-CNT Nanocomposites (Step 3).

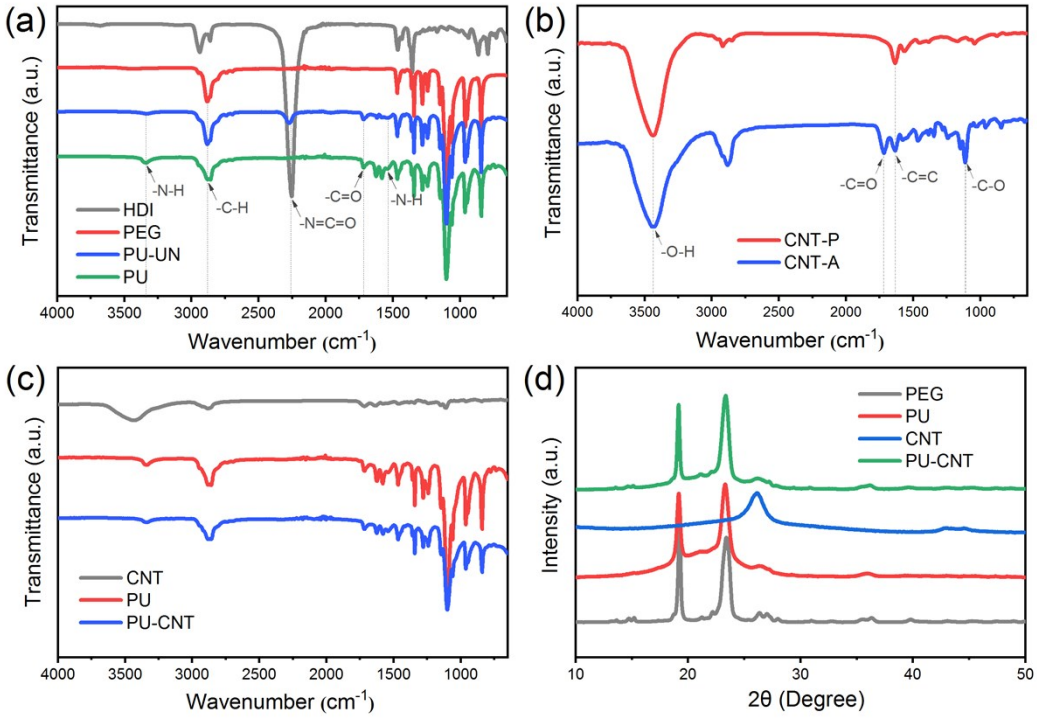

Figure S1. The structural characterization. FTIR spectrum of (a) PEG, HDI, PU, and PU-UN, (b) CNT-P and CNT-A, and (c) CNT, PU, and PU-CNT composite. (d) XRD patterns of PEG, PU, CNT, and PU-CNT composite.

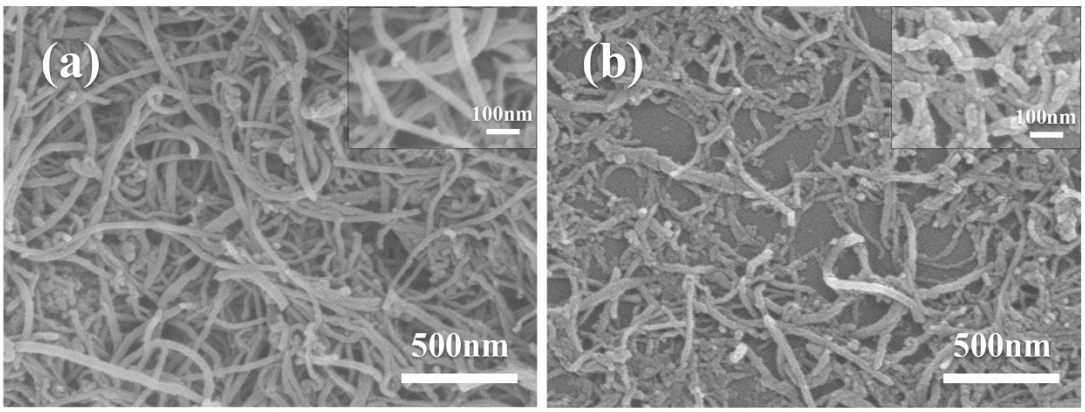

Figure S2. The SEM image of (a) CNT-P and (b) CNT-A.

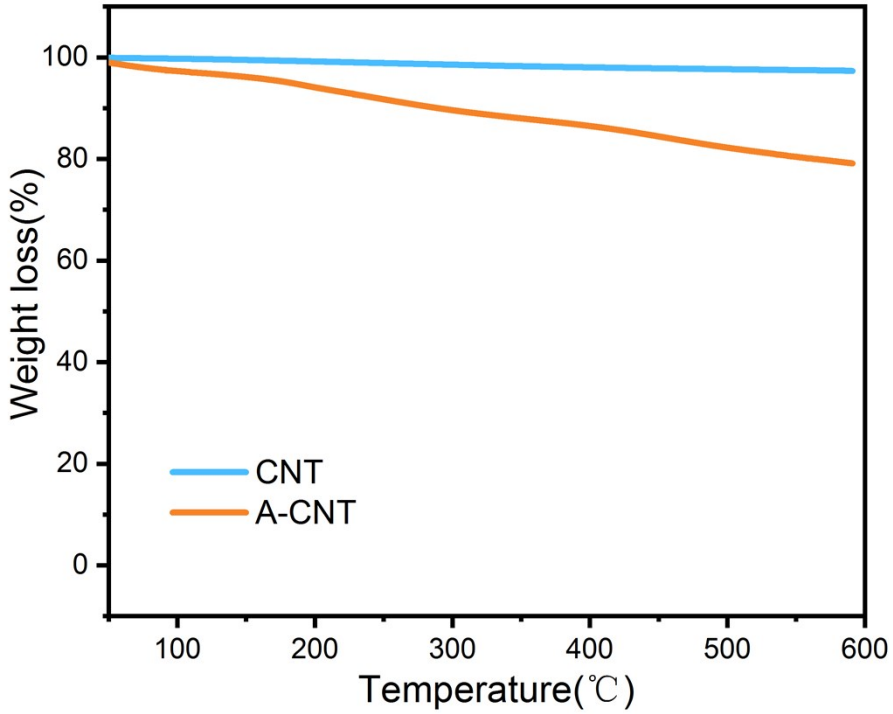

Figure S3. The TGA thermograms of CNT and A-CNT.

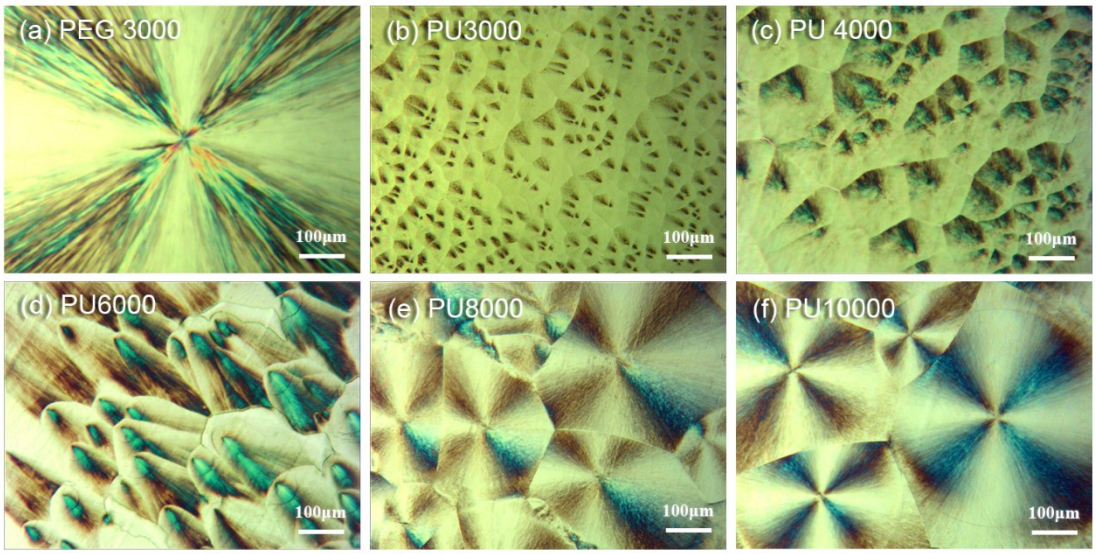

Figure S4. The POM image of (a) PEG3000; (b) PU3000; (c) PU4000; (d) PU6000; (e) PU8000; (f) PU10000.

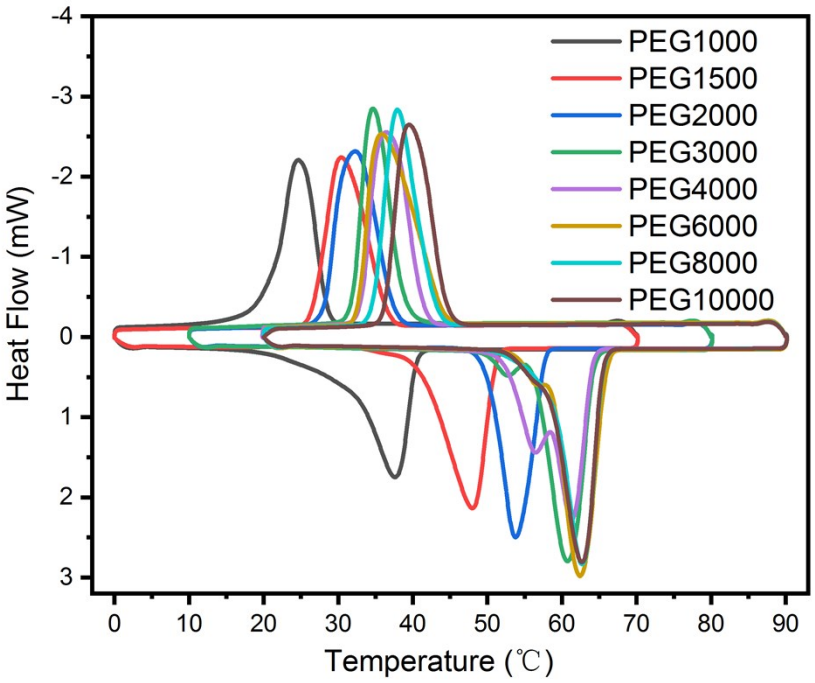

Figure S5. The DSC curves of PEG with different molecular weight

Table S1. Phase change behavior of PEG with different molecular weight

sample	T_p (°C) [a)]		ΔH ($J \cdot g^{-1}$) [b)]	
	Heating	Cooling	Heating	Cooling
PEG1000	31.3	28.3	152.7	145.1
PEG1500	43.5	37.8	154.6	149.8
PEG2000	50.4	37.3	163.6	157.2
PEG3000	50.3	38.3	171.8	160.4
PEG4000	52.5	41.0	173.7	160.8
PEG6000	54.4	43.8	174.3	161.9
PEG8000	59.0	43.9	174.8	163.6
PEG10000	59.3	44.1	175.1	164.4

[a)] T_p : phase change temperature; [b)]ΔH : phase change enthalpy

Table S2. Phase change behavior of PU samples with different PEG molecular weight.

sample	T_p (°C) [a]		Δ H (J·g^{-1}) [b]	
	Heating	Cooling	Heating	Cooling
PU1000	1.3	2.5	34.2	29.0
PU1500	21.3	17.5	52.8	44.9
PU2000	32.5	23.8	64.8	58.3
PU3000	39.1	31.4	78.0	71.4
PU4000	45.0	35.0	92.6	81.7
PU6000	46.3	37.5	105.2	94.1
PU8000	50.0	40.0	118.9	107.5
PU10000	55.0	42.5	143.1	131.9

[a] T_p : phase change temperature; [b] ΔH : phase change enthalpy

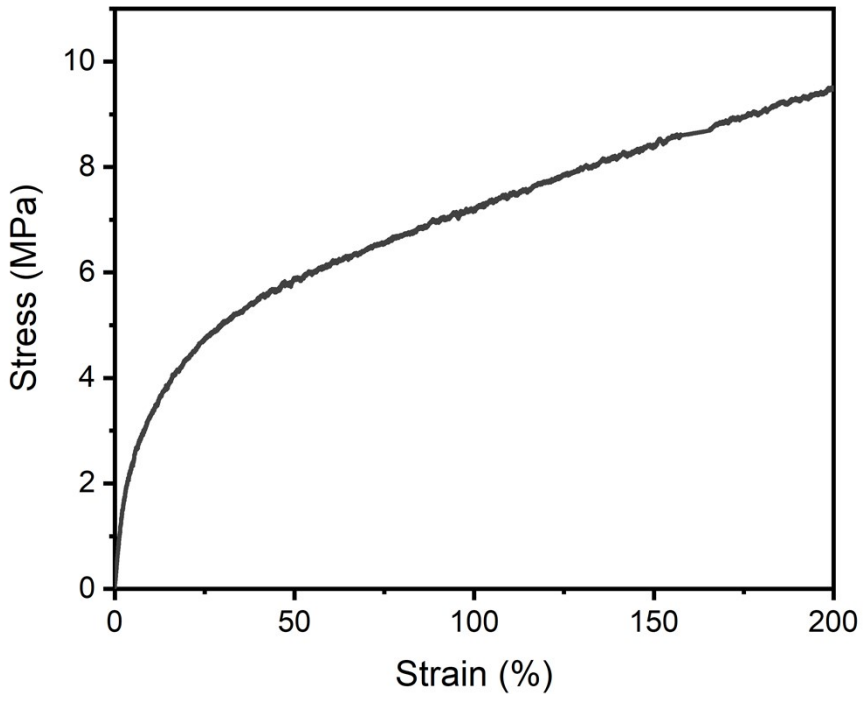

Figure S6. The stress and strain profiles of PU1000 sample

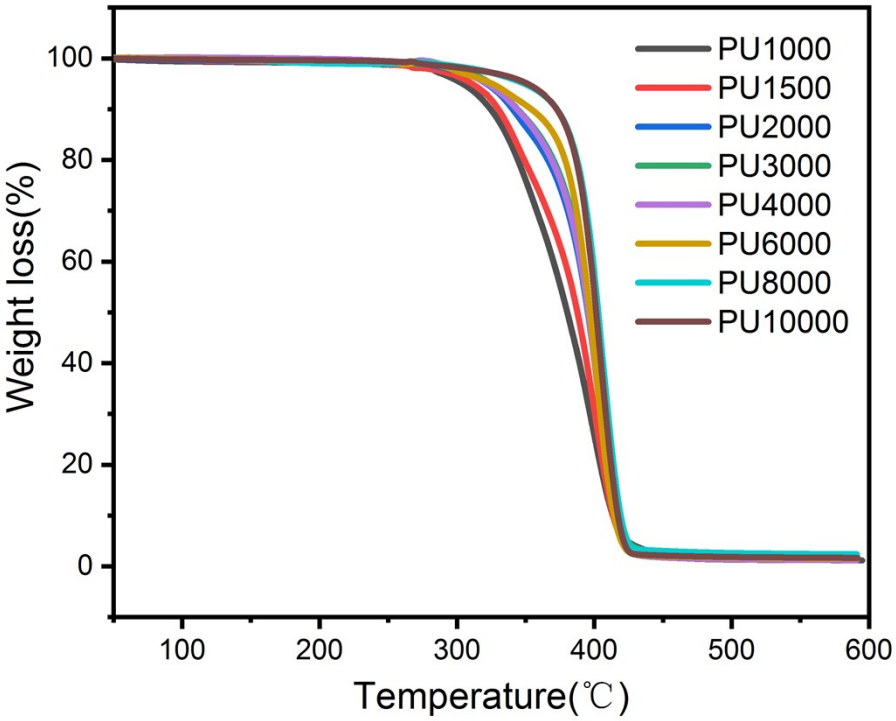

Figure S7. The TGA thermograms of PU samples with different PEG molecular weight.

Table S3. Phase change behavior of PU3000 and PU-CNT composites.

sample	T_p (°C) [a)]		ΔH ($J \cdot g^{-1}$) [b)]	
	Heating	Cooling	Heating	Cooling
PU3000	39.1	31.4	78.0	71.4
PU3000-CNT1	39.5	34.1	79.2	72.0
PU3000-CNT2	39.2	33.8	78.9	71.8
PU3000-CNT3	39.9	34.3	78.5	71.4

PU3000-CNT4	39.7	34.6	80.2	72.5
PU3000-CNT5	42.0	33.9	85.9	75.9

a) T_p : phase change temperature; [b)]ΔH : phase change enthalpy

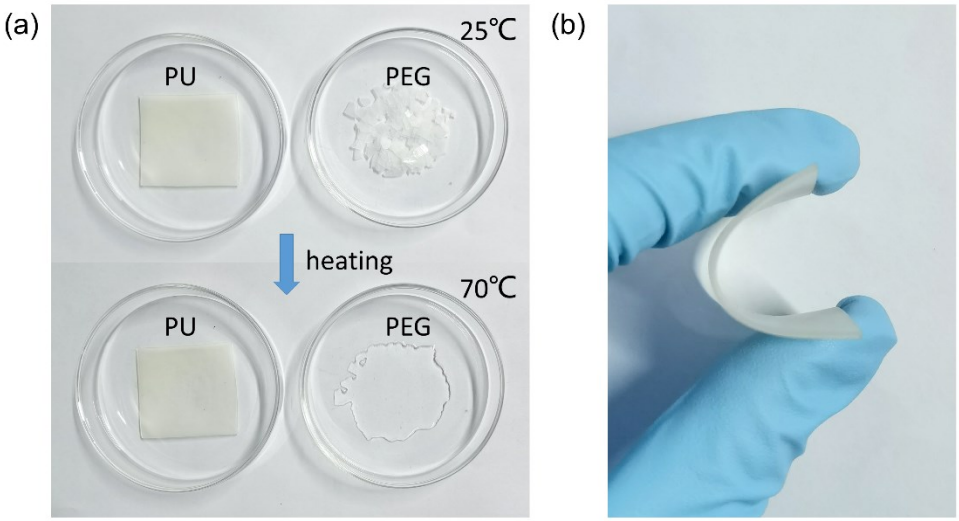

Figure S8. (a) Optical images of the pure PU3000 sample and PEG3000 before and after heating: at 70 °C, PU sample still remained solid state while PEG 3000 had become melting state, showing the solid-solid phase transition property of the pure PU. (b) Optical images of the pure PU3000 sample under curling condition, representing the flexibility and shape deformability of the pure PU sample.

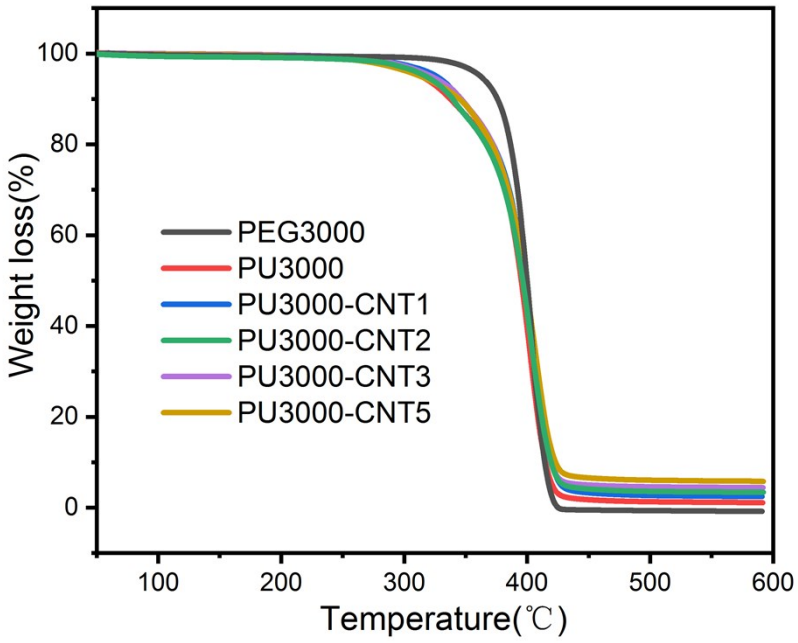

Figure S9. The TGA thermograms of PEG, PU, and PU-CNT composites.

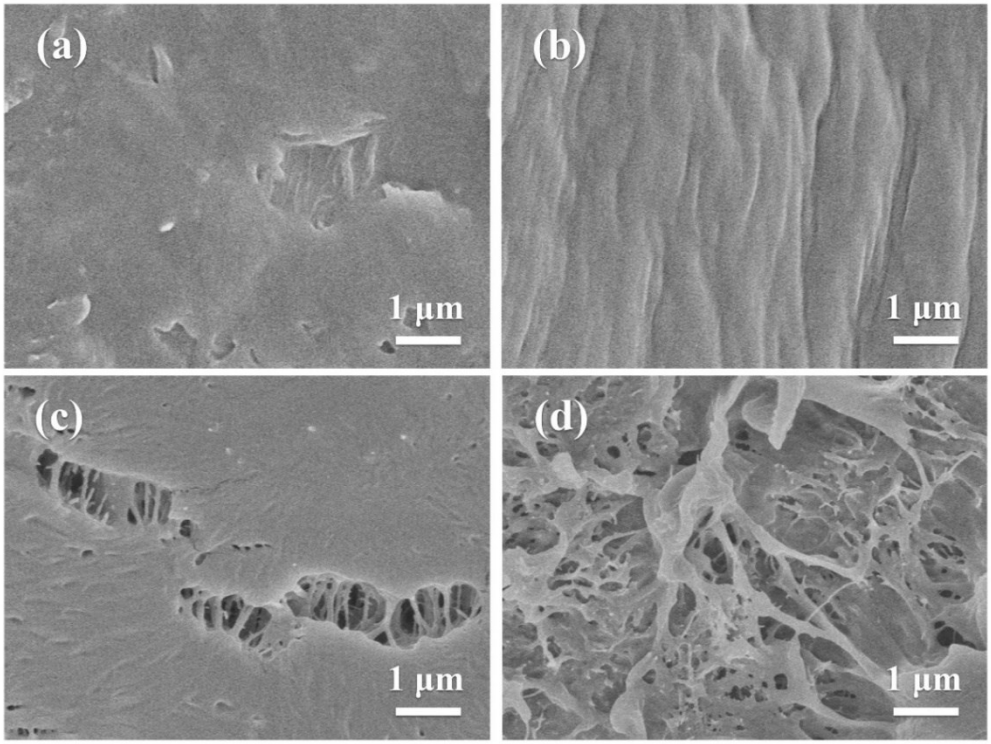

Figure S10. The SEM image of (a) the surface of PU; (b) the cross-section of PU; (c) the surface of PU-CNT composite; (d) the cross-section of PU-CNT composite.

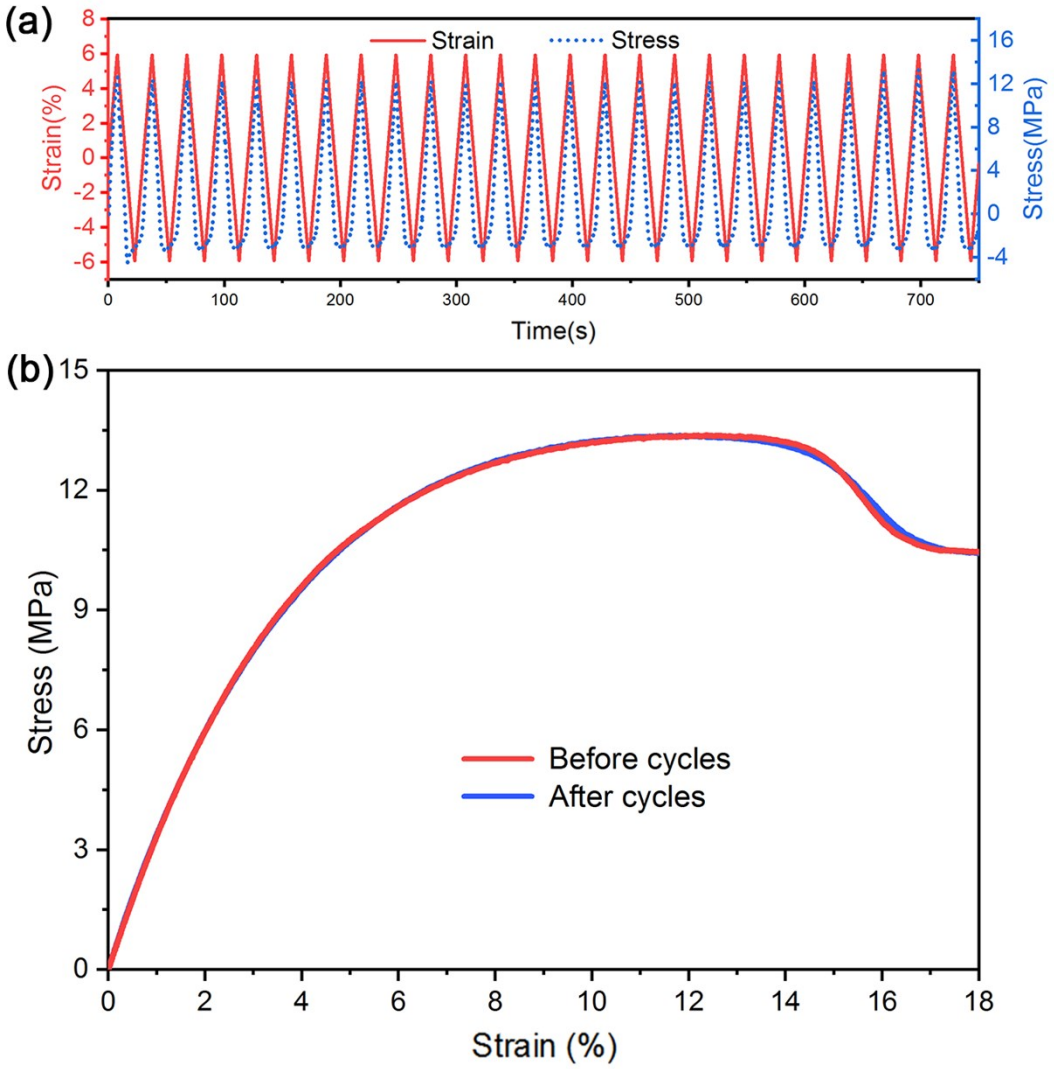

Figure S11. (a) The fatigue reliability test for the PU3000 sample with cyclic tensile stretch. (b) the strain-stress curve of the PU3000 sample after 25 tensile stretch cycles.

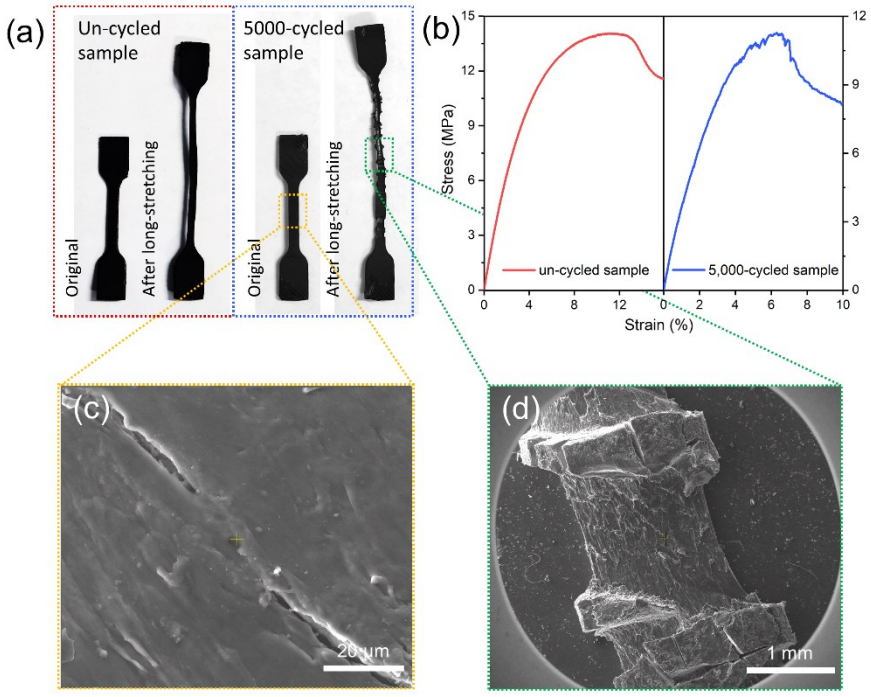

Figure S12. (a) The photograph of the original un-cycled sample and the un-cycled sample after long-stretching test (left), and the original 5,000 cycled sample and the 5,000 cycled sample after long-stretching test (right). (b) The long-stretching strain-stress curves of PU-CNT composite samples before and after 5,000 tensile stretch cycles, respectively. (c) The SEM image of the surface of PU-CNT composite after 5,000 tensile stretch cycles. (d) the SEM images of the 5,000 cycled sample after long-stretching test.

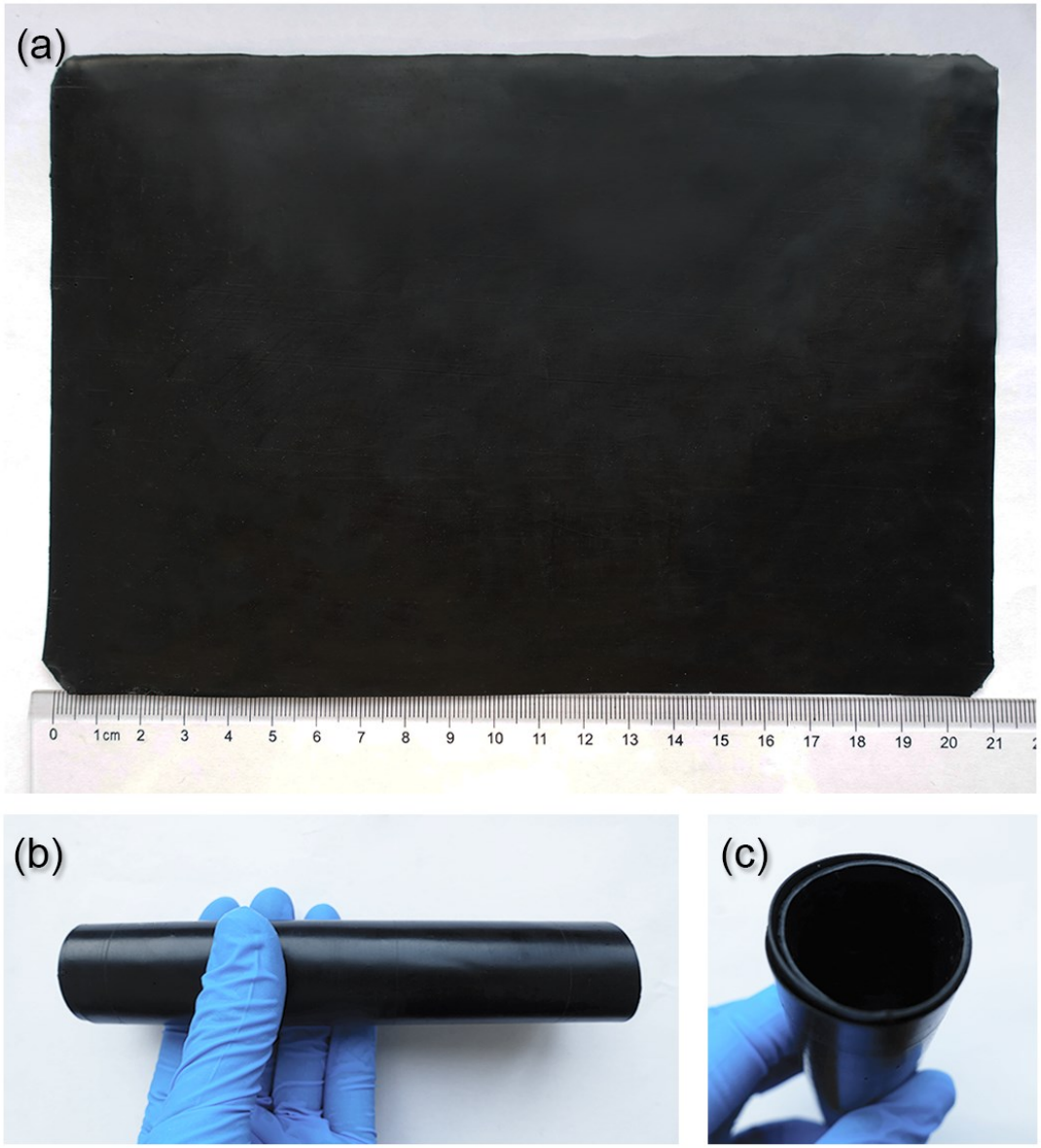

Figure S13. The large-scale preparation of this flexible PU-CNT composite films. (a) The photo of the large-scale sample with size of 21×15 cm^2; (b) front view and (c) top view of the large-scale sample under curling.

Table S4. The comparison of the thermal and mechanical performance of the currently reported flexible PCMs and the PU-CNT composites.

Composite	PCM content	ΔH_m (J g^{-1})	Yield/ break point	Yield/break strength (MPa)	Flexible source	Ref.
graphene aerogel fiber/PEG/ fluorocarbon resin coating	83 wt%	124	1.52%	12.7	graphene aerogel	[1]
carbonized cotton cloth/ paraffin/TPU	49.25 wt%	93.56	~2.5%	1.94	cotton cloth	[2]
paraffin/OBC/EG	80 wt%	111.4	0.21	2.4 (48°C)	OBC	[3]
polyolefin elastomer (POE) /stearic acid	50 wt%	-	-	9	POE	[4]
paraffin/MWCNTs/PP fiber	80.97 wt%	103.26	-	-	PP fiber	[5]
Kevlar nanofiber aerogel films/PEG (200 μm)	94.3 wt%	162.9	22.2%;	2.85	Kevlar fiber	[6]
Ag@Kapok fiber/lauric acid	81 vol %	146.8	-	-	Kapok fiber	[7]
PEG/cellulose acetate (CA) fibers	30 wt%	30.18	~8.2%	~7	CA	[8]
cellulose-grafted-PA16/GN16	91 wt%	78	~1.8%	3.6	cellulose	[9]
polyurethane/CNT	97 wt%	78.5	10.5%	16.3	PCM itself	This work

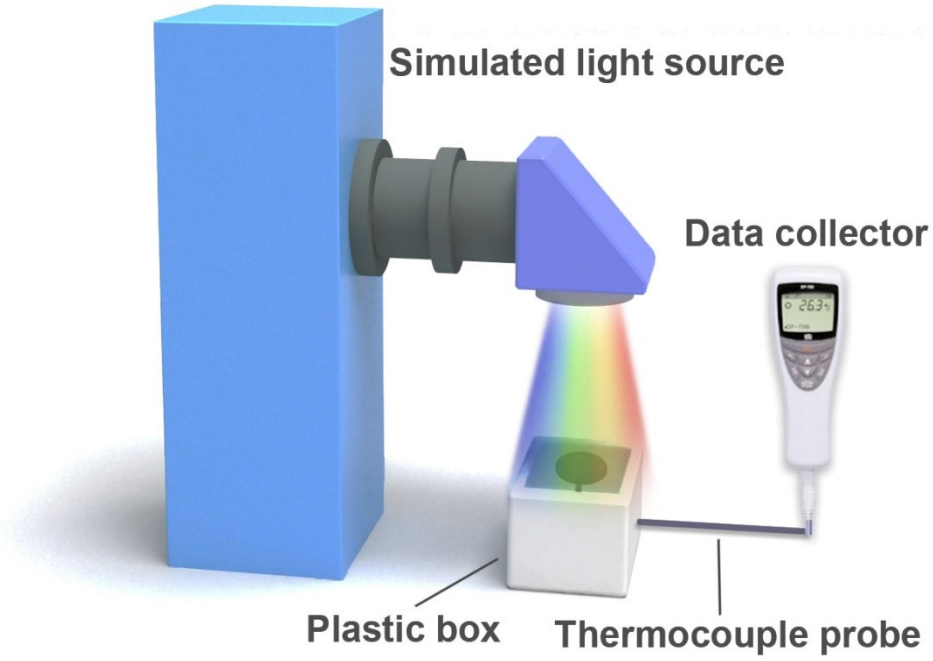

Figure S14. Schematic illustration of the experimental setup for the photo-thermal conversion.

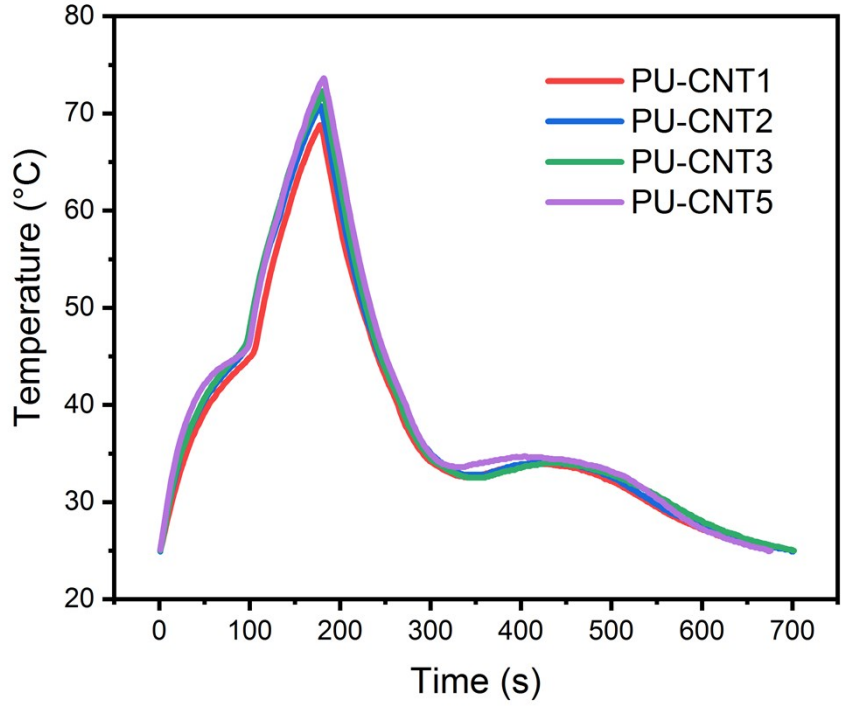

Figure S15. Time-temperature evolution curves of PU-CNT composites with increasing CNT wt. content

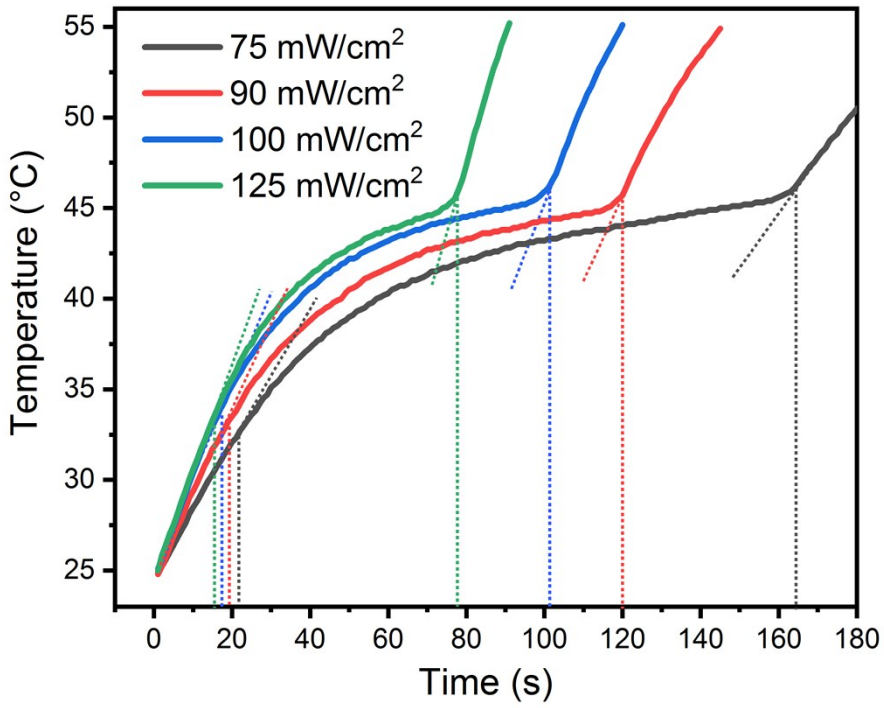

Figure S16. Evaluation of phase transition period as function of increasing light intensity during solar charging of PU-CNT5 sample.

Table S5. Solar-thermal energy storage performance of PU-CNT5 sample under different light intensities

Light Power (mW/cm^2)	75	90	100	125
Start time of phase change (s)	21	19	17	15
End time of phase change (s)	165	120	101	78
Phase change duration (s)	144	101	84	63
Input energy (J)	13.716	11.544	10.668	10.001
Stored energy (J)	8.590	8.590	8.590	8.590
Energy storage efficiency (%)[a)]	62.63	74.41	80.52	85.89

[a)] The photo-thermal energy storage efficiency was calculated as $\eta=(m\cdot\Delta H)/(A\cdot P\cdot t)$, in which m is the mass of sample, ΔH is phase change enthalpy, A is the irradiated surface area of sample, P is the power (mW/cm^2) of irradiation light and t is time of phase change period. The phase change period was determined by tangential method. In this case, A = 1.27 cm^2, m = 0.10 g, ΔH = 85.90 $J\cdot g^{-1}$

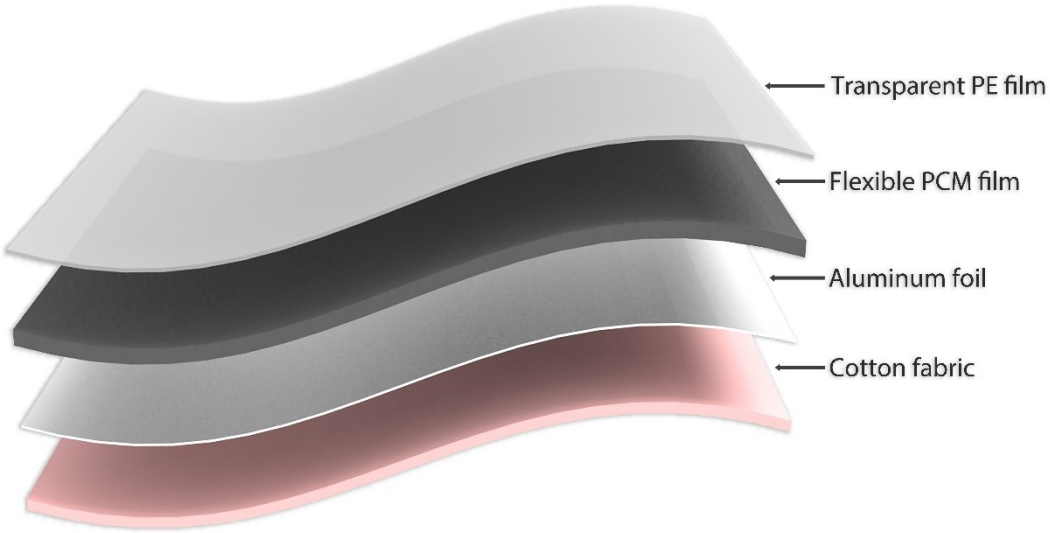

Figure S17. Schematic illustration of product composition for the photo-thermal human body management.

References

1. G. Li, G. Hong, D. Dong, W. Song and X. Zhang, *Advanced Materials*, 2018, **30**, 1801754.
2. M. M. Umair, Y. Zhang, S. Zhang, X. Jin and B. Tang, *Journal of Materials Chemistry A*, 2019, **7**, 26385-26392.
3. W.-W. Li, W.-L. Cheng, B. Xie, N. Liu and L.-S. Zhang, *Energy Conversion and Management*, 2017, **149**, 1-12.
4. J. Du, D. Liu, Z. Zhang, X. Yao, D. Wan, H. Pu and Z. Lu, *Polymer*, 2017, **126**, 206-210.
5. D. Luo, F. Wei, H. Shao, L. Xiang, J. Yang, Z. Cui, S. Qin and J. Yu, *Journal of Materials Science*, 2018, **53**, 15500-15513.
6. J. Lyu, Z. Liu, X. Wu, G. Li, D. Fang and X. Zhang, *ACS Nano*, 2019, **13**, 2236-2245.
7. S. Song, T. Zhao, W. Zhu, F. Qiu, Y. Wang and L. Dong, *ACS Applied Materials & Interfaces*, 2019, **11**, 20828-20837.
8. C. Chen, L. Wang and Y. Huang, *Applied Energy*, 2011, **88**, 3133-3139.
9. Y. Qian, N. Han, Z. Zhang, R. Cao, L. Tan, W. Li and X. Zhang, *ACS Applied Materials & Interfaces*, 2019, **11**, 45832-45843.